An in situ near-ambient pressure X-ray Photoelectron Spectroscopy study of CO_2 reduction at Cu in a SOE cell

Benedetto Bozzini[1]*, Matteo Amati[2], Claudio Mele[1], Axel Knop-Gericke[3] and Erik Vesselli[4]

[1]Dipartimento di Ingegneria dell'Innovazione, Università del Salento, via Monteroni s.n., 73100 Lecce, Italy

[2]Elettra - Sinctrotrone Trieste S.C.p.A. S.S. 14, km 163.5 in Area Science Park, 34149 Trieste-Basovizza, Italy

[3]Abteilung Anorganische Chemie, Fritz-Haber-Institut der Max-Planck Gesellschaft, Faradayweg 4–6, 14195 Berlin (Germany)

[4]Department of Physics, University of Trieste, via Valerio 2, I-34127 Trieste, Italy &
IOM-CNR, Laboratorio TASC, Area Science Park, S.S. 14 km 163.5, I-34149 Basovizza (Trieste), Italy

*Corresponding author: benedetto.bozzini@unisalento.it

ABSTRACT

The cathodic behavior of a model solid oxide electrolysis cell (SOEC) has been studied by means of near-ambient pressure (NAP) X-ray Photoelectron Spectroscopy (XPS) and near edge X-ray absorption fine structure (NEXAFS), aiming at shedding light on the specific role of the metallic component in a class of cermets used as electrodes. The focus is on the surface chemistry and catalytic role of Cu, the increasingly popular metallic component in electrodes used in CO_2 electrolysis and CO_2/H_2O co-electrolysis. The NAP-XPS and NEXAFS results, obtained in situ and operando conditions and under electrochemical control have provided important insights about the evolution of the Cu surface chemical composition. We have found that in dry CO_2 ambient carbon deposits are scavenged at low cathodic potential by the oxidising action of nascent O, while at high cathodic polarisations C grows due to activation of the CO reduction. Instead, in CO_2/H_2O mixtures, surface deposit of C is steady over the whole investigated potential range. The presence of adsorbed CO has also been detected during electrolysis of CO_2/H_2O mixtures, while no CO is found in pure CO_2 ambient.

KEYWORDS: CO_2 electrolysis; Cu; solid-oxide cell; near-ambient pressure XPS; NEXAFS

1. Introduction

Reduction of CO_2 to CO, a crucial step in the synthesis of hydrocarbons, is feasible by both chemical and electrochemical routes, though at high energetic costs. In the realm of electrochemistry, room- and high-temperature methodologies have been proposed, based on diverse electrolytes: aqueous, non-aqueous, molten-salt and solid oxides. In particular, CO_2 electrolysis and CO_2/H_2O co-electrolysis in solid-oxide electrolysis cells (SOECs) are attractive approaches. The high operating temperatures, typically divided in two ranges: intermediate (500÷700°C) and high (800÷1000°C), facilitate reaction kinetics, so that the use of noble metals can be avoided. Nevertheless intermediate-T operation is more desirable for durability issues as well as for the possibility of employing metallic cell supports with notably less severe brittleness problems, but still this is a field that has not been sufficiently explored.

The achievements of CO_2 electrolysis in SOECs have been the object of comprehensive recent reviews (e.g. [1-4]) as well as of a dedicated Faraday Discussion [5] and it is not necessary to repeat this information here, since our study is focused specifically on the role of metallic Cu constituent in SOECs cathodes. In order to place the role of Cu in context, it is worth recalling briefly the materials that have been used for CO_2-reduction SOECs: (i) Pt/YSZ [6-8]; (ii) Ni/YSZ [9-11]; (iii) ceria [12, 13]; (iv) Ni/GDC (Gd-doped ceria) [14, 15], Ni-Ru/GDC [15]; (v) Cu/YSZ [16-18]; (vi) Cu-doped La-Sr-Co-ferrite (LSCF)/CGO [19, 20]; (vii) Cu/GDC [21, 22]; (viii) La-Sr-Cr manganite(LSCM)-based p-type perovskites (LSCM/YSZ [11, 23], LSCM/GDC [11, 24]); Ni- [25] and Fe- impregnated LSCN [26]) and (ix) La-Sr titanate (LST)-based n-type perovskites, either in pure form [27] or Ni-impregnated [28]. Notwithstanding the rather extensive literature corpus, no general agreement has been reached regarding the best catalytic material for CO_2 reduction; in particular, there is still no consensus on the performance of the popular Ni-based cathodes, that are however recognized to exhibit a range of operational problems during CO_2 reduction. In this scenario Cu is gaining attention as an alternative to Ni owing to its resistance to coke formation and oxidation in hydrocarbon-fueled SOFCs [29, 30], as well as for cost reasons (Cu price is 25÷50% less than Ni). In fact, Cu is attractive on the one hand owing to its high current conductivity in both metallic [30] and cermet forms [31] and on the other hand for its catalytic activity towards CO_2 reduction, that has been shown to be similar to that of Ni [20,

21]. However, due to its lower melting temperature compared to Ni, Cu is not suitable for operation at temperatures higher than ca. 800°C due to tendency to particle coarsening.

Cu cermets have been considered as anodes for hydrocarbon oxidation in SOFC, showing outstanding resistance to deactivation due to C deposition and S poisoning, as well as good catalytic activity [30, 32, 33], but coarsening raises durability issues. Bimetallic Cu-Ni and Cu-Co SOFC anodes have also been tested, showing improved resistance to C deposition and crack formation as well as better catalytic performance [34-37]. In particular, outstanding performance of the CH_4/air SOFC was attributed to the optimal catalytic activity of Cu/CeO_2 for CH_4 due to the combination of the redox activity of the Ce^{4+}/Ce^{3+} couple with the high electronic conductivity of Cu [36, 37]. The use of Cu-containing SOFC anodes has not been restricted to applications involving C-containing fuels, but it has also been reported for H_2 oxidation [38, 39].

In addition to use of Cu in SOFC systems, a few very promising reports have been published regading CO_2 reduction. This has been first demonstrated for a peculiar SOFC configuration [19], where CO_2 reacted at the Cu-added $La_{0.58}Sr_{0.4}Co_{0.22}Fe_{0.8}O_{3-\square}$/CGO cathode, while H_2 was oxidised at a Ni/GDC anode. The first report comparing SOEC for CO_2 reduction, operated in CO_2/CO=1/1 at 750°C with Cu- and Ni-based cathodes, showed improved performance and stability [21]. Post mortem Raman studies following CO_2 or H_2O electrolysis and the CO_2+H_2O co-electrolysis at 550÷700°C using $Cu/Ce_{0.8}Gd_{0.2}O_{2-\square}$ (GDC), confirmed the suppression of C deposition [22]. Ni-Cu nanoparticles have been shown to combine the advantages of Ni and Cu, yielding a synergistic effect to maximise the current efficiencies for the direct electrolysis of CO_2. [40]. Cu/YSZ cathodes have also been used for H_2O electrolysis at 800°C, featuring comparable performance with Ni/YSZ electrodes [16-18]. Here we should mention the recent electrochemical study of CO_2 electrolysis and CO oxidation in CO_2/CO mixtures on Ce oxide electrodes patterned on YSZ using surface sensitive near ambient pressure XPS, very relevant to our investigations [13]. Operating the cell at 600°C they identified CO_3^{2-}as the key reaction intermediate, its formation being accompanied by Ce^{3+}/Ce^{4+} valence changes. It is noteworthy that no other in situ XPS work has been publihsed so far of CO_2 electrolysis: as a result the surfece chemistry of Cu-containing systems in these conditions is a fully unexplored topic, whose

contribution will be crucial in clarifying mechanistic aspects related to C- deposition and durability of cathodes.

The aim of this study is to shed light on some fundamental aspects of the surface electrochemistry of Cu-based systems, in particular on the specific role of Cu in the recently proposed highly active Cu/GDC cathodes [21, 22]. To this end – as a model system that as such has not been considered in actual SOEC studies – we explored the evolution of the status of Cu thin film electrodes in contact with YSZ during the CO_2 reduction reaction by near-ambient pressure (NAP) XPS and NEXAFS complemented by electrochemical measurements of two-probe linear sweep voltammetry (LSV) and electrochemical impedance spectroscopy (EIS), detailed in [41].

2. Experimental Methods

2.1. Cell fabrication

In the present investigation, we employed planar, YSZ(100)-supported cells with lithographically defined Cu (working electrode) and Mn (counter electrode) thin-film electrodes. We used pure Cu in order to avoid the chemical complexities of cermets from which Cu particles are obtained by partial reduction (see e.g. [40]). Even though studies on planar solid-oxide cells exposed to just a single reactive gas are not identical to those on real SOECs in which the fuel and the oxidant are separately brought into contact with optimised, highly-active working and counter electrodes, nevertheless mechanistic information gathered from this type of study is directly related to the relevant electrodic processes. The specific cell rationale, geometry, electrode fabrication and electrochemical characterisation have been detailed in a dedicated paper [41]. Over the years, we have developed lithographed planar cells for in situ micro-XPS in view of two main objectives: (i) to render the whole electrochemical system (cathode, electrolyte and anode) accessible to the X-ray beam; (ii) to confine the region exhibiting the highest electrochemical activity to the surface, to which of course XPS is uniquely sensitive. At variance with the more traditional stacked electrode configurations with porous electrodes (e.g. [42]), in our planar lithographed cells the electrochemically active triple-phase boundaries are provided by the contact lines between electrode and electrolyte, exposed to the gas ambient of the

analysis chamber. The choice and behaviour of the counter-electrode is detailed in [41]. Cu has been selected as the cathode in order to be able to single out the contribution of this element to the cathodic operation of the Cu-based cermets recalled in the Introduction. YSZ(100) single crystals (1 cm × 1 cm × 1 mm) were obtained from Mateck and used as cell support. The electrodes were fabricated by evaporating 70 nm thick Cu and Mn layers onto Au (30 nm) contact layers, in turn grown onto Cr adhesion buffers (10 nm): Figure 1a shows the electrode arrangement and dimensions. In order to achieve a high surface density of triple phase boundaries (TPB) with the lithographic approach and to expose a significant length of TPB lines to the probe beam (ca. 150 μm in diameter), the electrodes were designed with a square lattice of circular holes (4 □m in diameter), giving access to the YSZ. The electrolysis cell is placed inside the XPS chamber on a suitable sapphire sample-holder (Figure 1b) equipped with proper electrical connections and a laser heater, capable of reaching high temperatures.

2.2. Electrochemical methods

Linear sweep voltammetry (LSV) and electrochemical impedance spectrometry (EIS) measurements in two-electrode configuration were performed in the analysis chamber at the working temperature in gas environment. We employed a Versastat potentiostat and data were acquired with the Versastudio software. For compactness of presentation, all through the paper, we shall refer to voltage with its absolute cell value, considering that the Cu and Mn patches have always been polarised cathodically and anodically, respectively.

2.3 Near-ambient pressure XPS and NEXAFS

Pristine cells were initially exposed to 0.5 mbar of either CO_2 or CO_2/H_2O 1:1 at room temperature and subsequently they were brought to the operating temperature of 600°C. Subsequently the gas environment was changed, at the same pressure, from CO_2/H_2O 1/1 ambient to CO_2/H_2O 1/2. We explored the cathodic behaviour of Cu in CO_2 and CO_2/H_2O gas ambient, following the potential-dependent evolution of the Cu 2*p*, O 1*s* and C 1*s* core levels and Cu L-edge and O K-edge NEXAFS spectra. The experiments were carried out at the ISISS beamline of the BESSY-II Synchrotron in Berlin [43]. Since the experimental set-up using applied potentials interferes with the measurement of the sample currents as well as with the secondary electron signal, NEXAFS spectroscopy was performed by following the changes of the XPS and Auger

signal while scanning the photon energy. Thus, the XPS and NEXAFS spectra probe comparable sample depths, relevant exclusively to the surface and near-surface chemical states. The XPS signal was calibrated with respect to the Au 4*f* reference. Peak deconvolution of the O 1*s* and C 1*s* XPS spectra was performed by least-squares fitting of the normalised and energy-calibrated signal with Doniach-Šunjić lineshapes, convoluted with a Gaussian envelope and with the addition of a linear background [44]. A non-symmetric lineshape was used also in the deconvolution of the core levels of adsorbed species at the metal surface. Indeed, at low kinetic energies the contribution of inelastic scattering processes (extrinsic losses) may significantly deviate the lineshape with respect to a pure Voigt profile, at variance with isolated atoms and molecules. Furthermore, beyond the sudden, single electron approximation, the creation of a core hole in an atomic species at a metal surface gives origin to shake-up and shake-off features that, accompanied by unresolved vibrational losses of the adiabatic peak, may also indirectly contribute to an apparent asymmetry of the adiabatic spectroscopic line [45, 46]. Energy calibration was performed with respect to the OCP value.

3. Experimental Results

The potential-dependent cathodic surface electrochemistry of Cu films forming a TPB with YSZ electrolyte and a reactive gas phase was investigated by NAP XPS and NEXAFS in two representative environments of SOEC operation: CO_2 electrolysis and CO_2/H_2O co-electrolysis. Spectroscopy measurements were carried out potentiostatically. The first set of experiments studied CO_2 electrolysis, operating the cell at three cell voltages: OCP, 2 and 4 V. In the second experimental set a pristine cell was sequentially exposed to CO_2/H_2O ambient at 1/1 and 1/2 ratios and polarised at 2 V for a total period of 28 hours in each case.

Figure 1c compares SEM micrographs of the Cu electrode in pristine conditions and at the end of the experiments in CO_2 ambient. The SEM morphology of the cathode after measurements in CO_2/H_2O is essentially the same as after operation in dry CO_2. For both gas environments the main degradation forms are extensive pitting within the Cu patch and diffusion of metal into the electrolyte region, as one can notice from the compositional contrast in the YSZ regions of the pristine and aged cells. As mentioned in the

Introduction, diffusion and agglomeration of Cu have been reported to be typical damaging modes of Cu-containing cermets used in both SOFCs [33, 38] and SOECs [21].

3.1 Electrochemical measurements

Full details of the electrochemical measurements can be found in our previous paper [41]. Here we briefly recapitulate the essential linear sweep voltammetry (LSV) information. It is worth noting that, owing to the special nature of our TPB geometry and the reproducibility of the geometry ensured by the lithographic fabrication, it is more significant to refer to the cell current than to the current density. Figure 2 reports LSVs measured with pristine cells. The data obtained in CO_2 indicate mixed control and a secondary inhibition process can be noticed from the feature highlighted with a star at ca. 1.2 V, the voltage required for the oxidation of C adsorbed at the Cu cathode under OCP (see also Figure 4b below). In pure H_2O, significantly higher currents are measured due to the higher H_2O reactivity, coherently with previous results [22] showing that at a given current density steam electrolysis at Cu/GDC requires lower voltages than CO_2 reduction. The LSV behavior in CO_2/H_2O=1/1 has contributions from both reduction reactions and no changes in slope are observed that could be related to C desorption.

3.2. In situ XPS and NEXAFS

3.2.1. CO_2 electrolysis - Figure 3a shows Cu 2*p* spectra recorded in 0.5 mbar CO_2 at OCP followed by two successive cathodic polarisations of 2 and 4 V. The Cu $2p_{3/2}$ binding energy is centred at 931.9 eV: a peak position that is compatible with both Cu^0 and Cu^+ species [47]. However, the presence of the shake-up features at ca. 938 and 945 eV unambiguously indicates the formation of Cu_2O. These in-situ XPS spectra are in concert with post mortem Raman [22] and XRD [21] analyses of Cu-containing SOEC cathodes after CO_2 electrolysis, reporting the presence of Cu_2O in their Cu/GDC. The changes in the Cu 2*p* intensity upon switching the cell potential (Figure 3b) are due to the variations in the C amount deposited on the surface, which, as judged from the C 1*s* spectra, reaches the lowest level at 2 V, as reported in Figure 3b where the C 1*s* intensities are obtained from the spectra in Figure 4b.

The O 1*s* spectra, shown in Figure 4a consist of at least two distinct components. At open-circuit, two peaks can be clearly separated at 530.0 ± 0.1 and 531.5 ± 0.1 eV, shifting to 529.6 ± 0.1 and 530.9 ± 0.1 eV, respectively, when applying the potential. It is worth noting that, as detailed in [41], we operated in a way that ensures that spectral shifts are not due to charging effects resulting from the application of the electrochemical polarisation. The peak at 530.9 eV is compatible with the presence of Cu_2O [47-49] and its intensity correlates with that of the Cu shake-up features of Figure 3a. The peak at 531.5 eV present at OCP conditions could be in principle attributed also to several overlapping C-O forms like for example $CO_2^{\delta-}$ [49]. However, this latter assignment may be valid only in the case of the OCP spectrum, since it can be definitely ruled out for the biased samples due to the too low binding energy and to the absence of signal in the corresponding C 1*s* spectra (Figure 4b), thus making the contribution from Cu_2O the most plausible interpretation. The role of hydroxyl species is also excluded since OH is not expected to be stable up to 600°C [50], and a significant OH surface coverage may be obtained only when in equilibrium with the water gas phase (see Section 3.2.2 below). The most likely interpretation for the peak at 529.6-530.0 eV consists instead in attributing it to atomic oxygen species, either chemisorbed [47-49] or in subsurface form [48]. This scenario is coherent with the more general one recently set by XPS studies with high lateral resolution of the oxidation process of metal surfaces in reactive ambient, that has pinpointed high surface heterogeneities, typically characterised by the coexistence of different oxidation states [51]. In this framework, the shift observed between OCP conditions and after the application of the cathodic polarisation is fully compatible - both qualitatively and quantitatively - with surface reconstruction or faceting as well as with thickness variations of the oxide layer.

Figure 4b reports the C 1s spectra. The dominant feature at 283.9 eV can be attributed to atomic or carbidic carbon [52]. Interestingly, and in line with the corresponding Cu 2*p* spectra (Figure 3a), no carbidic carbon is present at 2 V, while at 4 V a carbon deposit forms, similarly to OCP conditions. Minor changes in peak position and shape between the spectra measured at OCP and at 4 V do not warrant a different spectral assignment; in fact, the C 1*s* line position originating from atomic carbon species is known to shift by a few

tenths of eV, depending on the reaction conditions and the surrounding chemical environment. This effect, according to the literature, can be attributed to coadsorption and local restructuring phenomena, while any type of chemical bonding, a fortiori to oxygen, would yield a chemical core level shift that is larger by an order of magnitude [53]. Moreover, it is worth noting that switching back to OCP (top spectrum in panel b of Figure 4) a carbon deposit is again present, even though the corresponding C 1s peak is significantly smaller with respect to the initial conditions. The absence of carbon deposits at 2V is a result that is in keeping with [13]. Graphitic C, present at OCP, is removed under oxidising conditions due to both segregation and the direct reaction of pre-adsorbed carbon with oxygen in the supporting oxide at the electrolyte surface, while at the metal surface an electrode-cleaning procedure based on oxidation of the metal surface by CO_2 dissociation takes place. After elimination of the carbon deposit present at the initial OCP, two small features appear at 293.3 eV and 296.2 eV, assigned to K $2p_{3/2}$ and $2p_{1/2}$, respectively. K is indeed a typical trace element of the YSZ electrolyte [54], accessible to analysis through the holes of the electrode patches (see Figure 1). According to the interpretation above, K traces become visible upon segregation to the surface of the oxide after removal of the initial adventitious carbon contamination.

Figure 5 shows Cu-L and O-K NEXAFS spectra obtained in the Auger yield mode. The spectra contain multiple features, that correspond to well-known species and can be readily assigned by means of a qualitative comparison with the published data [47, 55-58]. For the present purpose, we reckon that it is adequate to carry out this comparison by simply marking the energy positions of the key features corresponding to the reported species. As far as the Cu L spectra are concerned, the position of the L_3 edge at 933.5 eV, together with the feature at 954.0 eV (L_2, separation of 20.5 eV) and the peak at 937.0 eV unequivocally reveal the coexistence of Cu^0 and Cu^+ phases. We suppose that the metallic Cu component is present due to probing depth larger than the thickness of the thin oxide layer or disruption of the top oxide layer so the underlying metallic Cu contributes to the signal as well. In particular, the L_3 and L_2 features are related to the dipole transition of the Cu $2p_{3/2}$ and $2p_{1/2}$ electrons into the empty d-states and their energy separation is therefore determined by the spin-orbit coupling, which is known to be dependent on the oxidation state [55]. Concerning the O K edge the main feature at 532.3 eV indicates that the Cu_2O phase dominates [47, 55] and the copper oxide phase grows further with the reaction, since the corresponding

absorption features gain intensity after switching on the potential. However, the small pre-edge shoulder at ~531 eV can bear some contribution from chemisorbed O or non-stoichiometric CuO_x phase. All O K edge spectra show a broad structure in the 535-538 eV range that can be ascribed to gas-phase CO (feature at ca. 535.7 eV) and CO_2 (feature at ca. 537.1 eV) [56-58]. This assignment is further confirmed by the data collected simultaneously in the total yield mode (not reported, for brevity), emphasizing the gas-phase contribution. Interestingly, a contribution from a subsurface oxygen species that acts as an oxide precursor has been reported to contribute in this same range to the near-edge spectra and therefore cannot be excluded [59]. Notwithstanding these observed strong gas-phase contributions to the O K edge spectra, the features of Cu_2O can be however reliably ascertained, as reported in the previous reference.

3.2.2.CO_2/H_2O co-electrolysis - The Cu 2*p* XPS spectra recorded in 0.5 mbar CO_2/H_2O 1/1 and 1/2 (not reported, for brevity) are essentially the same as observed in pure CO_2 where the Cu_2O phase was found to be formed. Compared to the case of pure CO_2 the O 1*s* spectra are somewhat different. As can be seen in Figure 6a at OCP the atomic oxygen component dominates in the 529.9-530.3 eV range, shifting to higher binding energies for higher applied potential, thus indicating an increased oxidation of the surface. In parallel, a weaker feature is present at OCP at 531.5 eV, shifting up to 531.8 eV at increasing bias. Based on previous literature data [49], it is hardly possible to assign unequivocally this latter feature to a single chemical species. In particular, apart from the OCP spectrum, its binding energy is too high for bulk Cu oxide phases, while it may be compatible with $CO_2^{\delta-}$ and/or OH moieties. Since the intensities were normalised to the background, it is evident that keeping constant the CO_2/H_2O ratio, both components grow by increasing the applied cathodic polarisation. However, comparing the spectra of Figure 6a with the evolution of the O 1*s* spectra taken in pure CO_2 ambient (Figure 4a), it is evident that the component assigned to Cu_2O remains dominant in both cases. If the CO_2/H_2O ratio is brought to 1/2 at 2 V, the intensity ratio changes in favour of the higher-binding energy component, compatibly with a contribution to the latter from OH species.

Compared to the pure CO_2 ambient, C 1*s* spectra in the case of CO_2 + H_2O co-electrolyses contain new components (Figure 6b), in analogy with the O 1*s* region. A clear shoulder at higher binding energy with respect to the main peak can already be noticed under the initial OCP conditions. Deconvolution shows two

peaks at 283.7±0.1 and 285.2±0.1 eV, respectively. The lower-binding energy feature corresponds to the single peak present in pure CO_2 ambient, while the higher-binding energy one can be assigned to CO [52, 60]. These are the only C-containing species that can be assigned on the basis of spectroscopic data. We cannot exclude that other products form, but surely they do not contribute to the surface composition, that is the scope of this work. It is worth noting that it is customary in NAP-XPS studies of high-surface area catalysts, to monitor the gas phase of the analysis chamber by mass spectrometry: in the present case this was not possible owing to the fact that the low active surface of our planar, lithographed electrodes did not allow to achieve an appropriate signal-to-noise ratio for meaningful speciation. It is apparent that the dependence of carbon coverage on the potential is profoundly affected by the presence of H_2O: while in pure CO_2 the initial carbon contamination (0 V – OCP) disappears at 2 V, when the Cu electrode is exposed to the reactant mixture (CO_2/H_2O) the C 1*s* peak is still present and it decreases with the applied voltage. It is worth noting that the intensity of the higher-binding energy shoulder is notably less affected by the applied potential and it remains almost constant. Essentially the same scenario is found for both the investigated CO_2/H_2O ratios. As discussed below, this should be ascribed to a process involving a water/hydrogen-assisted mechanism that efficiently promotes the fast decomposition of carbon dioxide at the surface of the electrode either as a result of H_2 formation from H_2O decomposition or by direct reaction with H_2O [60]. At the end of the experiment, C removal was attempted in pure H_2O ambient at 0.5 mbar, performing a series of potentiostatic experiments by increasing the cell voltage in steps of 1 V and holding the potential for 5 min, until a significant reduction of the C 1*s* peak intensity was observed at 5 V. Figure 7 reports the potential dependent C 1*s* spectra and a representative selection of potentiostatic transients, showing a straightforward correlation between the cell current and the amount of adsorbed C. It can be clearly seen that at 5 V, a distinct increase of cell current is recorded, corresponding to the reductive desorption of C from the cathode, correlated with a clear decrease of the C 1*s* peak intensity

NEXAFS spectra at the Cu L and O K edges, measured under CO_2+H_2O co-electrolysis (Figure 5b) do not add qualitatively new information since the same characteristic features were found as in CO_2 ambient. The Cu L spectra are identical to those measured in CO_2 (Figure 5a) and have been omitted for brevity, while the

O K ones (Figure 5c) simply indicate a more strongly oxidised surface, coherently with the foregoing discussion.

4. Discussion

4. 1. CO_2 electrolysis

Our *in situ* results regarding CO_2 electrolysis suggest the reaction scenario detailed below and marshalled into Figure 8. The Cu electrode surface in the initial conditions (0 V – OCP) is fairly oxidised and covered with adventitious carbon. When a cathodic polarisation of 2 V is applied, CO_2 decomposition sets in, yielding CO+O. During this reaction, that is an oxidising one [29], the produced atomic oxygen at the electrode surface reacts: (i) with the initially pre-adsorbed carbidic species to CO, as evidenced by the disappearance of the C 1*s* peak of the atomic carbon species when switching the potential from OCP to 2 V and (ii) with the electrode surface, yielding Cu_2O, as witnessed by the growth of the oxide-related features observed in the Cu and O NEXAFS and XPS spectra. It is known that, in order to dissociate CO_2 on copper, a barrier of 1.5÷1.7 eV has to be overcome [61], while CO decomposition requires a higher energy (about 2.5 eV). Apparently at 2 V the CO dissociation cannot compete with the low-barrier CO desorption, favoured at the operating cell temperature of 600°C. Thus at 2 V the electrode surface is already oxidised and carbon cannot accumulate. However, when the potential is increased to 4 V, also CO dissociation becomes feasible and carbon accumulation at the surface occurs. No signal from adsorbed species (carbonate, carbon monoxide, carbon dioxide) is observed and it is in fact not expected due to the high surface temperature (600 °C) at which the residence time of both reactants and products is known to be very short, thus yielding negligible surface coverage values. For completeness, it is worth reporting here that the joint analysis of the C 1*s* and O 1*s* peaks recorded at 600°C in CO_2 0.5 mbar at ceria cathodes in [13] has been explained with the presence of carbonate - with possibly some contribution to the O 1*s* spectrum from the SiO_2 support - in a wide range of electrochemical conditions. The adsorption of CO_x species at ceria [62, 63], ceria/copper and Cu [64] had been previously reported to be unstable above ambient temperature.

4.2. CO_2/H_2O co-electrolysis

The presence of a surface CO peak in the C 1*s* XPS spectra measured during the CO_2+H_2O co-electrolysis can be explained with the fact that water reduction, that occurs at significantly lower voltages than CO_2 reduction on Cu (see e.g. [22]), yields hydrogen that may assist CO_2 reduction to CO. In addition, even at OCP conditions, direct interaction between CO_2 and water molecules at the catalyst surface can also lower the CO_2 decomposition barrier, as previously observed under both model and near-ambient pressure conditions [52, 60]. Indeed, a hydrogen-assisted mechanism can lower the energy barrier for the CO_2 dissociation into CO and O so as to make it a fast process even at very low temperature [60]. Further reduction of CO, enabled by the increased rate of hydrogen production resulting from the applied cathodic polarisation, stabilises the surface coverage with carbidic carbon also at 2 V, where C is instead oxidised in pure CO_2 ambient. This scenario is further supported by the intensity changes of the O 1*s* peak measured with applied polarisation.

5. Conclusions

In this paper we have studied in situ and operando the surface chemistry of a Cu cathode under CO_2 electrolysis and CO_2/H_2O co-electrolysis conditions by near ambient pressure XPS and NEXAFS in a model SOEC at 600°C. Our key findings are that in dry CO_2, pre-existing C deposits are scavenged at lower cathodic potential (cell voltage of 2 V) by the oxidising action of nascent oxygen resulting from CO_2 reduction, while C forms at the cathode surface at higher cathodic polarisations (cell voltage of 4 V) as a result of the reduction of CO, which is not activated at the lower voltages. In dry CO_2 no surface C-O species are found, while in CO_2/H_2O adsorbed CO is present as a result of CO_2 reduction favoured by H_2 formation, resulting from H_2O decomposition or by direct reaction with water. Under co-electrolysis conditions, due to the presence of adsorbed CO, C deposits are stabilised and can be reacted off only at significantly more reducing potentials.

Acknowledgments

The authors gratefully acknowledge the beamtime at BESSY II provided by the Helmholtz-Zentrum-Berlin.

References

[1] M.A. Laguna-Bercero, Recent advances in high temperature eelctrolysis using solid oxide fuel cells: A review, J. Power Sources 2034 (2012) 4-16.

[2] Ph. Moçotéguy, A. Brisse, A Review and Comprehensive Analysis of Degradation Mechanisms of Solid Oxide Electrolysis Cells, Int. J. Hydrogen Energy 38 (2013) 15887-15902.

[3] S.D. Ebbesen, S.H. Jensen, A. Hauch and M.B. Mogensen, High Temperature Electrolysis in Alkaline Cells, Solid Proton Conducting Cells, and Solid Oxide Cells, Chem. Rev. 114 (2014) 10697-10734.

[4] L. Bi, S. Boulfrad and E. Traversa, Steam electrolysis by solid oxide electrolysis cells (SOECs) with proton-conducting oxides, Chem. Soc. Rev., 43 (2014) 8255-8270.

[5] "Solid Oxide Electrolysis: Fuels and Feedstocks from Water to Air" University of York (UK), 13-15 July 2015. Faraday Discussions 182 (2015).

[6] K. R. Sridhar and B. T. Vaniman, Oxygen production on Mars using solid oxide electrolysis, Solid State Ionics 93 (1997) 321-328.

[7] G. Tao, K.R. Sridhar, C.L. Chan, Study of carbon dioxide electrolysis at electrode/electrolyte interface: part I. Pt/YSZ interface, Solid State Ionics 175 (2004) 615–619.

[8] G. Tao, K.R. Sridhar, C.L. Chan, Study of carbon dioxide electrolysis at electrode/electrolyte interface: part II. Pt-YSZ cermet/YSZ interface2 Solid State Ionics 175 (2004) 621–624.

[9] S.D. Ebbesen, M. Mogensen, Electrolysis of carbon dioxide in Solid Oxide Electrolysis Cells, J. Power Sources, 193 (2009), 349–358.

[10] C. Graves, S.D. Ebbesen, M. Mogensen, Co-electrolysis of CO_2 and H_2O in solid oxide cells: performance and durability, Solid State Ionics 192 (2011) 398–403.

[11] X. Yue and J. T. S. Irvine, Alternative Cathode Material for CO_2 Reduction by High Temperature Solid Oxide Electrolysis Cells, J. Electrochem. Soc., 159 (2012) F442–F448.

[12] R. D. Green, C.-C. Liu and S. B. Adler, Carbon dioxide reduction on gadolinia-doped ceria cathodes, Solid State Ionics, 179 (2008) 647–660.

[13] Y. Yu, B. Mao, A. Geller, R. Chang, K. Gaskell, Z. Liu and B.W. Eichhorn, CO_2 activation and carbonate intermediates: an operando AP-XPS study of CO_2 electrolysis reactions on solid oxide electrochemical cells, Phys.Chem.Chem.Phys. 16 (2014) 11633-11639.

[14] P. Kim-Lohsoontorn, N. Laosiripojana, J. Bae, Performance of solid oxide electrolysis cell having bi-layered electrolyte during steam electrolysis and carbon dioxide electrolysis, Curr. Appl.Phys. 11 (2011) S223–S228.

[15] P. Kim-Lohsoontorn, J. Bae, Electrochemical performance of solid oxide electrolysis cell electrodes under high-temperature coelectrolysis of steam and carbon dioxide, J. Power Sources 196 (2011) 7161–7168.

[16] S. Lee, K.H. Kang, J.M. Kim, H.S. Hong, Y. Yun, S.K. Woo, Fabrication and characterization of Cu/YSZ cermet high-temperature electrolysis cathode material prepared by high-energy ball-milling method I. 900°C-sintered, J. Alloy Compd 448 (2008) 363–367.

[17] S. Lee, J.M. Kim, H.S. Hong, S.K. Woo, Fabrication and characterization of Cu/YSZ cermet high temperature electrolysis cathode material prepared by high-energy ball-milling method II. 700°C-sintered, J. Alloy Compd 467 (2009) 614–621.

[18] J. Kim, S. Lee, K.H. Kang, H.S.Hong, Preparation and characterization of Cu/YSZ cathode for high-temperature electrolysis, Int. J. Energy Res. 34 (2010) 438–444.

[19] T.J. Huang, C.L. Chou, Electrochemical CO_2 reduction with power generation in SOFCs with Cu-added LSCF–GDC cathode, Electrochem. Commun. 11 (2009) 1464–1467.

[20] T.J. Huang, X.D. Shen, C.L. Chou, Characterization of Cu, Ag and Pt added $La_{0.6}Sr_{0.4}Co_{0.2}Fe_{0.8}O_{3-\square}$ and gadolinia-doped ceria as solid oxide fuel cell electrodes by temperature-programmed techniques, J. Power Sources 187 (2009) 348–355.

[21] C.-Y. Cheng, G. H. Kelsall and L. Kleiminger, Reduction of CO_2 to CO at Cu–ceria-gadolinia (CGO) cathode in solid oxide electrolyser, J. Appl. Electrochem. 43 (2013) 1131–1144.

[22] C. Gaudillere, L. Navarrete, J.M. Serra, Syngas production at intermediate temperature through H_2O and CO_2 electrolysis with a Cu-based solid oxide electrolyzer cell, Int. J. Hydrogen Energy 39 (2014) 3047-3054.

[23] F. Bidrawn, G. Kim, G. Corre, J. T. S. Irvine, J. M. Vohs and R. J. Gorte, Efficient Reuction of CO_2 in a Solid Oxide Elerctrolyzer, Electrochem. Solid-State Lett., 11 (2008) B167–B170.

[24] X. Yue and J. T. S. Irvine, Impedance studies on LSCM/GDC cathode for high temperature CO_2 electrolysis, Electrochem. Solid State Lett. 15 (2012) B31–B34.

[25] Y. Li, Y. Gan, Y. Wang, K. Xie, Y. Wu, Composite cathode based on Ni-loaded $La_{0.75}Sr_{0.25}Cr_{0.5}Mn_{0.5}O_{3-\delta}$ for direct steam electrolysis in an oxide-ion-conducting solid oxide electrolyzer, Int. J. Hydrogen Energy 38 (2013) 10196–10207.

[26] S. Xu, S. Chen, M. Li, K. Xie, Y. Wang, Y. Wu, Composite cathode based on Fe-loaded LSCM for steam electrolysis in an oxide-ion-conducting solid oxide electrolyser, J. Power Sources 239 (2013) 332–340.

[27] S. Li, Y. Li, Y. Gan, K. Xie, G. Meng, Electrolysis of H_2O and CO_2 in an oxygen-ion conducting solid oxide electrolyzer with a $La_{0.2}Sr_{0.8}TiO_{3-\delta}$ composite cathode, J. Power Sources 218 (2012) 244–249.

[28] Y. Gan, Q. Qin, S. Chen, Y. Wang, D. Dong, K. Xie, Y. Wu, Composite cathode $La_{0.4}Sr_{0.4}TiO_{3-\delta}$-$Ce_{0.8}Sm_{0.2}O_{2-\delta}$ impregnated with Ni for high-temperature steam electrolysis, J. Power Sources 245 (2014) 245–255.

[29] S. Park, J.M. Vohs & R.J. Gorte, Direct oxidation of hydrocarbons in a solid-oxide fuel cell, Nature 404 (2000) 265-267.

[30] A. Atkinson, S. Barnett, R.J. Gorte, J.T.S. Irvine, A.J. McEvoy, M. Mogensen, S.C. Singhal and J. Vohs, Advanced anodes for high-temperature fuel cells, Nature materials 3 (2004) 17-27.

[31] J. Tartaj, V. Gilb, A. Mourea, Low-temperature preparation by polymeric complex solution synthesis of Cu–Gd-doped ceria cermets for solid oxide fuel cells anodes: Sinterability, microstructures and electrical properties, J. Power Sources 195 (2010) 2800–2805.

[32] Z. Zhan, S.I. Lee, Thin film solid oxide fuel cells with copper cermet anodes, J. Power Sources 195 (2010) 3494–3497.

[33] L. Zhao, X. Ye, Z. Zhan, High-performance cathode-supported solid oxide fuel cells with copper cermet anodes, J. Power Sources 196 (2011) 6201–6204.

[34] A. Fuerte, R.X. Valenzuela, M.J. Escudero, L. Daza, Effect of cobalt incorporation in copper-ceria based anodes for hydrocarbon utilisation in Intermediate Temperature Solid Oxide Fuel Cells, J. Power Sources 196 (2011) 4324–4331.

[35] X.-F. Ye, S.R. Wang, J. Zhou, F.R. Zeng, H.W. Nie, T.L. Wen, Application of a Cu–CeO_2/Ni–yttria-stabilized zirconia multi-layer anode for anode-supported Solid Oxide Fuel Cells operating on H_2–CO syngas fuels, J. Power Sources 196 (2011) 5499–5502.

[36] X. Meng, X. Gong, N. Yang, Y. Yin, X. Tan, Z.-F. Ma, Carbon-resistant Ni-YSZ/Cu-CeO_2-YSZ dual-layer hollow fiber anode for micro tubular solid oxide fuel cell, Int. J. Hydrogen Energy 39 (2014) 3879-3886.

[37] X. Meng, X. Gong, Y. Yin, N. Yang, X. Tan, Z.-F. Ma, Effect of the co-spun anode functional layer on the performance of the direct-methane microtubular solid oxide fuel cells, J. Power Sources 247 (2014) 587-593.

[38] N. Kiratzis, P- Holtappels, C.E. Hatchwell, M. Mogensen and J.T.S. Irvine, Preparation and Charecterization of Copper/Yttria Titania Zirconia Cermets for Use as Possible Solid Oxide Fuel Cell Anodes, Fuel Cells 1 (2001) 211-218.

[39] M.C. Tucker, G.Y. Lau, C.P. Jacobson, S.J. Visco, L.C. De Jonghe, Cu–YSZ cermet solid oxide fuel cell anode prepared by high-temperature sintering, J. Power Sources 195 (2010) 3119–3123.

[40] H. Wei, K. Xie, J. Zhang, Y. Zhang, Y. Wang, Y. Qin, J. Cui, J. Yan and Y. Wu,
In situ Growth of Ni_xCu_{1-x} Alloy Nanocatalysts on Redox-reversible Rutile $(Nb,Ti)O_4$ Towards High-Temperature Carbon Dioxide Electrolysis, Sci. Rep. 4 (2014) 5156 (11 pages).

[41] B. Bozzini, M. Amati, P. Bocchetta, S. Dal Zilio, A. Knop-Gericke, E. Vesselli and M- Kiskinova, An in situ near-ambient pressure X-ray Photoelectron Spectroscopy study of Mn polarised anodically in a cell with solid oxide electrolyte, Electrochim. Acta 174 (2015) 532-541.

[42] R. Arrigo, M. Hävecker, M.E. Schuster, C. Ranjan, E. Stotz, A. Knop-Gericke and R. Schlögl, In Situ Study of the Gas-Phase Electrolysis of Water on Platinum by NAP-XPS, Angew. Chem. Int. Ed. 52 (2013) 11660 –11664.

[43] https://www.helmholtz-berlin.de/pubbin/igama_output?modus=einzel&gid=1607
last accessed on June 6th, 2016

[44] S. Doniach, M. Sunjic, Many-electron singularity in X-ray photoemission and X-ray line spectra from metals, J. Phys. C 3 (1970) 285-291.

[45] B. Gumhalter, Line shapes and relaxation effects in core-level photoelectron spectra of chemisorbed species, Phys. Rev. B 19 (1979) 2018-2026.

[46] N. Mårtensson, A. Nilsson, Core-Level line shapes of adsorbates: effects of electronic and vibrational excitations, J. El. Spectrosc. Rel. Phen. 52 (1990) 1-46.

[47] P. Jiang, D. Prendergast, F. Borondics, S. Porsgaard, L. Giovanetti, E. Pach, J. Newberg, H. Bluhm, F. Besenbacher and M. Salmeron, Experimental and theoretical investigation of the electronic structure of Cu_2O and CuO thin films on Cu(110) using x-ray photoelectron and absorption spectroscopy, J. Chem. Phys. 138 (2013) 024704 (6 pages).

[48] H. Bluhm, M. Hävecker, A. Knp-Gericke, E. Kleimenov and R. Schlögl, D. Teschner, V.I. Bukhtiyarov, D.F. Ogletree and M. Salmeron, Methanol Oxidation on a Copper Catalyst Investigated Using in Situ X-ray Photoelectron Spectroscopy, J. Phys. Chem. B 108 (2004) 14340-14347.

[49] B. Eren, Ch. Heine, H. Bluhm, G.A. Somorjai and M. Salmeron, Catalyst Chemical State during CO Oxidation Reaction on Cu(111) Studied with Ambient- Pressure X‑ray Photoelectron Spectroscopy and Near Edge X-ray Adsorption Fine Structure Spectroscopy, J. Am. Chem. Soc. 137 (2015), 11186−11190.

[50] M.I. Mazharul, B. Diawara, V. Maurice, P. Marcus, First principles investigation on the stabilization mechanisms of the polar copper terminated Cu_2O(111) surface, Surf. Sci. 603 (2009) 2087-2095.

[51] R. Blume, M. Hävecker, S. Zafeiratos, D. Techner, A. Knop-Gericke, R. Schlögl, L. Gregoratti, A. Barinov and M. Kiskinova, Ruthenium Active Catalytic States: Oxidation States and Methanol Oxidation Reactions, Ch. 10 in RSC Nanoscience & Nanotechnology No. 19 "Nanostructured Catalysts - Selective Oxidations", Edited by Ch. Hess and R. Schlögl, Royal Society of Chemistry 2011, pp. 248-265.

[52] E. Vesselli, E. Monachino, M. Rizzi, S. Furlan, X. Duan, C. Dri, A. Peronio, C. Africh, P. Lacovig, A. Baldereschi, G. Comelli, and M. Peressi, Steering the Chemistry of Carbon Oxides on a NiCu Catalyst, ACS Catal. 3 (2013) 1555-1559.

[53] M. Roiaz, E. Monachino, C. Dri, M. Greiner, A. Knop-Gericke, R. Schlögl, G. Comelli and Erik Vesselli, Reverse Water–Gas Shift or Sabatier Methanation on Ni(110)? Stable Surface Species at Near-Ambient Pressure, J. Am. Chem. Soc. 138 (2016) 4146–4154.

[54] J.S. Becker, J. Westheide, A.I. Saprykin, H. Holzbrecher, U. Breuer and H.-J. Dietze. Mass Spectrometric Analysis of Ceramic Components for Solid Oxde Fuel Cells, Mikrochim. Acta 125 (1997) 153-160.

[55] A.B. Gurevich, B.E. Bent, A.V. Teplyakov, J.G. Chen, A NEXAFS investigation of the formation and decomposition of CuO and Cu_2O thin films on Cu(100), Surf. Sci. 442 (1999) L971-L976.

[56] O. Björneholm, A. Nilsson, E. Zdansky, A. Sandell, B. Hernnäs, H. Tillborg, J. Andersen, N. Mårtensson, 2π-resonance broadening in x-ray-absorption spectroscopy of adsorbed CO, Phys. Rev. B 46 (1992) 10353–10365.

[57] L. Triguero, L.G.M. Pettersson and H. Ågren, Calculations of near-edge x-ray-absorption spectra of gas-phase and chemisorbed molecules by means of density-functional and transition-potential theory, Phys. Rev. B 58 (1998) 8097-8110.

[58] O. Björneholm, A. Nilsson, E. Zdansky, A. Sandell, H. Tillborg, J. Andersen, N. Mårtensson, Higher excited states in x-ray-absorption spectra of adsorbates, Phys. Rev. B 47 (1993) 2308-2319.

[59] A. Knop-Gericke, M. Hävecker, T. Schedel-Niedrig, R. Schlögl, Probing the electronic structure of an active catalyst surface under high-pressure reaction conditions: the oxidation of methanol over copper, Catal. Lett. 66 (2000) 215-220.

[60] E. Vesselli, M. Rizzi, L. De Rogatis, X. Ding, A. Baraldi, G. Comelli, L. Savio, L. Vattuone, M. Rocca, P. Fornasiero, A. Baldereschi and M. Peressi, Hydrogen-Assisted Transformation of CO_2 on Nickel: The Role of Formate and Carbon Monoxide, J. Phys. Chem. Lett. 1 (2010) 402-406.

[61] A.A. Gokhale, J.A. Dumesic, M. Mavrikakis, On the Mechanism of Low-Temperature Water Gas Shift Reaction on Copper, J. Am. Chem. Soc. 130 (2008) 1402-1414.

[62] T. Staudt, Y. Lykhach, N. Tsud, T. Skala, K. C. Prince, V. Matolín and J. Libuda, Electronic Structure of Magnesia-Ceria Model Catalysts, CO_2 Adsorption, and CO_2 Activation: A Synchrotron Radiation Photoelectron Spectroscopy Study, J. Phys. Chem. C 115 (2011) 8716–8724.

[63] S. D. Senanayake, D. Stacchiola, J. Evans, M. Estrella, L. Barrio, M. Pérez, J. Hrbek and J. A. Rodriguez, Probing the reaction intermediates for the water–gas shift over inverse CeOx/Au(1 1 1) catalysts, J. Catal. 271 (2010) 392–400.

[64] K. Mudiyanselage, S. D. Senanayake, L. Feria, S. Kundu, A. E. Baber, J. Graciani, A. B. Vidal, S. Agnoli, J. Evans, R. Chang, S. Axnanda, Z. Liu, J. F. Sanz, P. Liu, J. A. Rodriguez and D. J. Stacchiola, Importance of the Metal–Oxide Interface in Catalysis: In Situ Studies of the Water–Gas Shift Reaction by Ambient-Pressure X-ray Photoelectron Spectroscopy, Angew. Chem., Int. Ed. 52 (2013) 5101–5105.

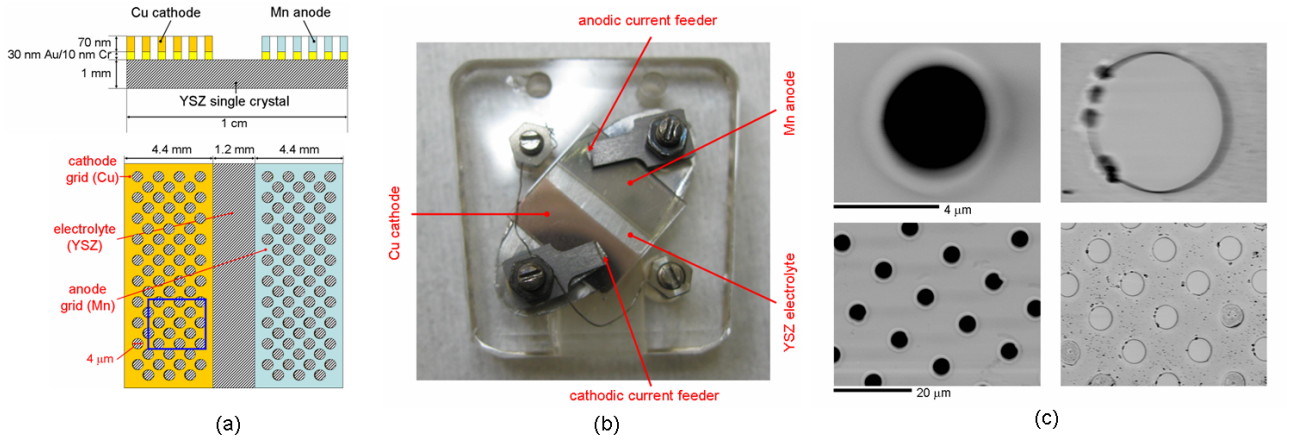

Figure 1 – (a) Sketch of the electrochemical cell: (top) planar view where the square indicates the area of SEM images; (bottom) cross-sectional view. (b) Cell mounted on sample holder and (c) Low and high resolution SEM images of a pristine cell (left) and after operation in CO_2 at 600°C (right).

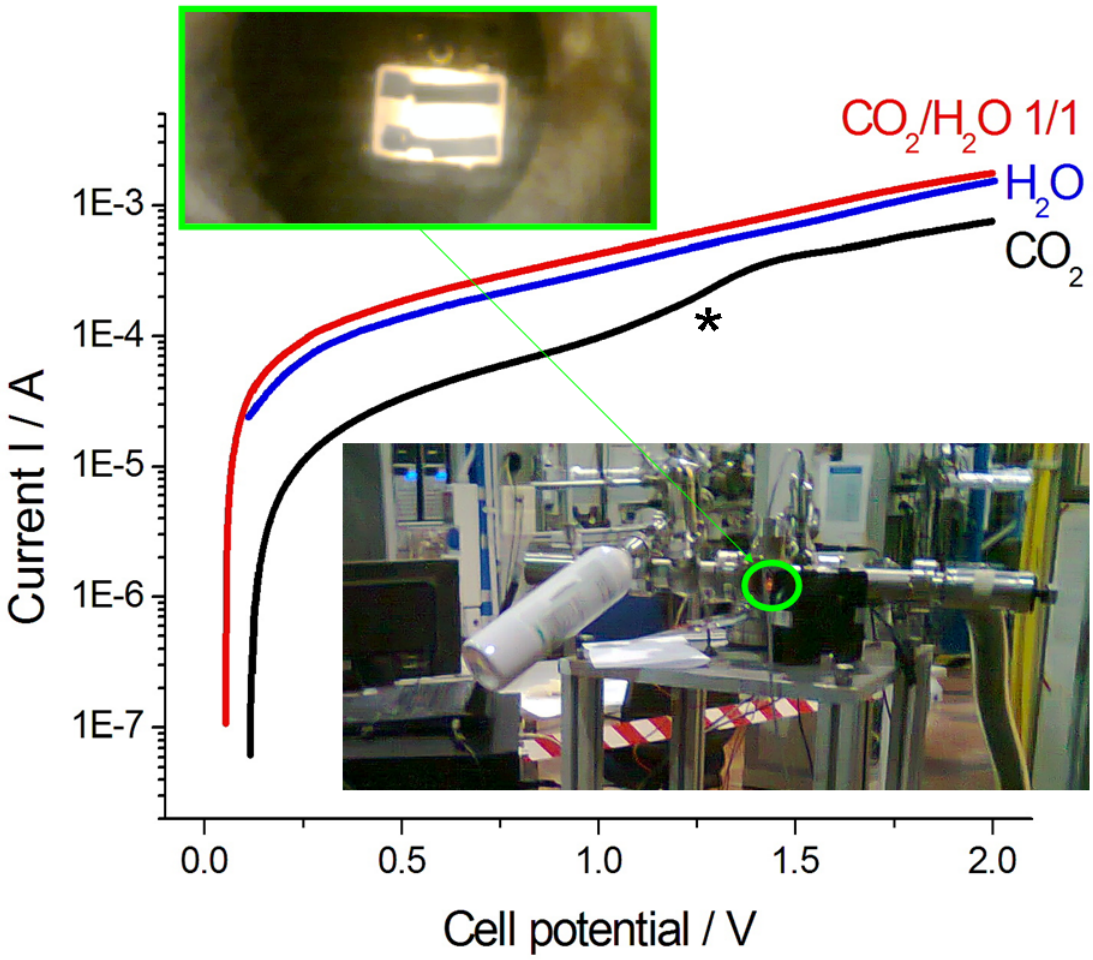

Figure 2 – Linear-sweep voltammograms of the Cu/YSZ/Mn cell, measured at 600°C, 0.5 mbar in the indicated gas ambient. The star denotes the potential range where secondary inhibition takes place. The figure also shows: the mock-up of the analysis chamber used for off-line electrochemical experiments (below) and the operating electrochemical cell imaged through the viewport (above).

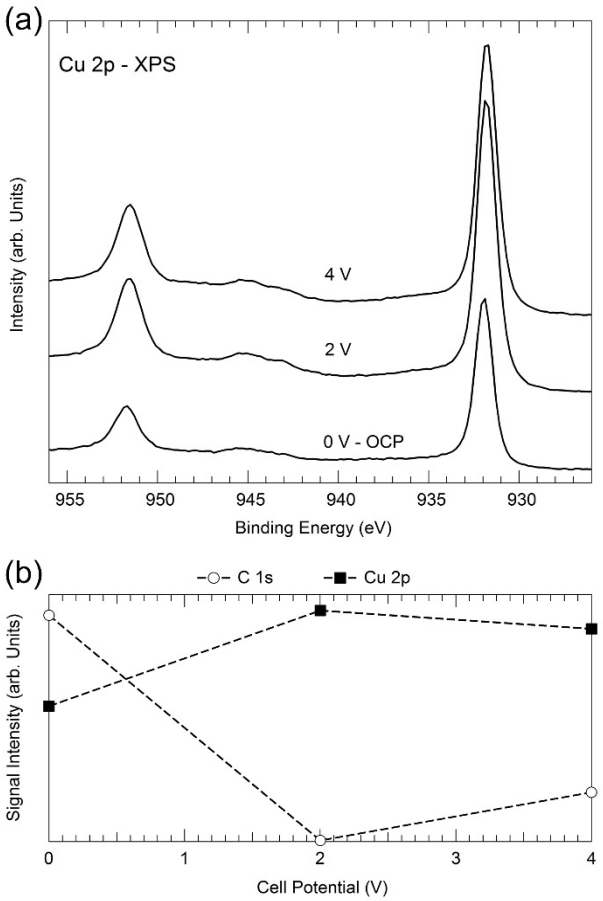

Figure 3 – (a) Cu 2*p* XPS spectra recorded in 0.5 mbar CO_2 at 600°C at the indicated potentials. (b) C 1*s* and Cu 2*p* XPS signal intensities, obtained from data plotted in Figures 4b and 3a, respectively.

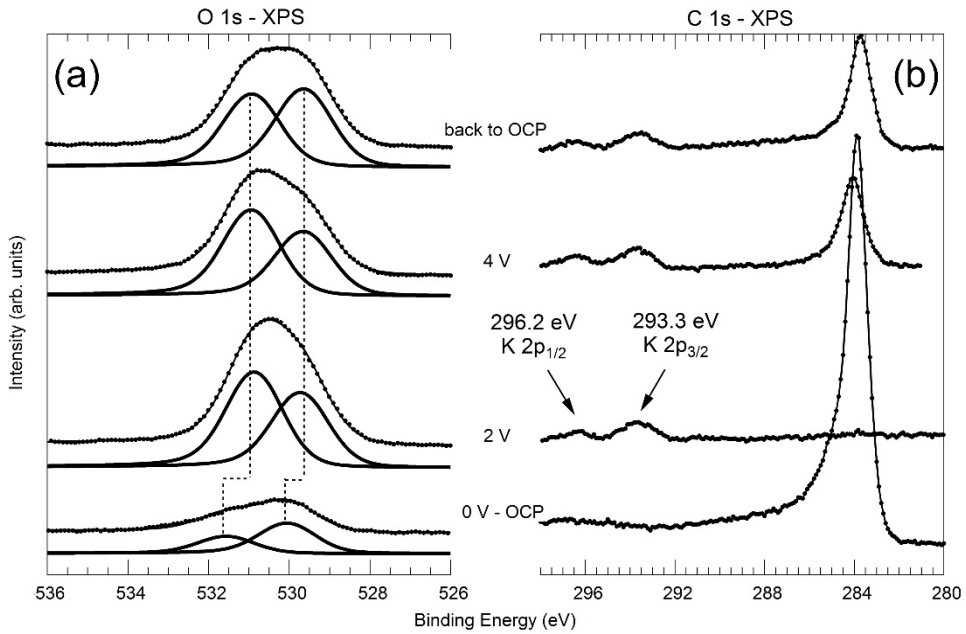

Figure 4 – (a) O 1*s* and (b) C 1*s* XPS spectra recorded in 0.5 mbar CO_2 at 600°C at the indicated potentials. The continuous lines are the results of the fitting procedure.

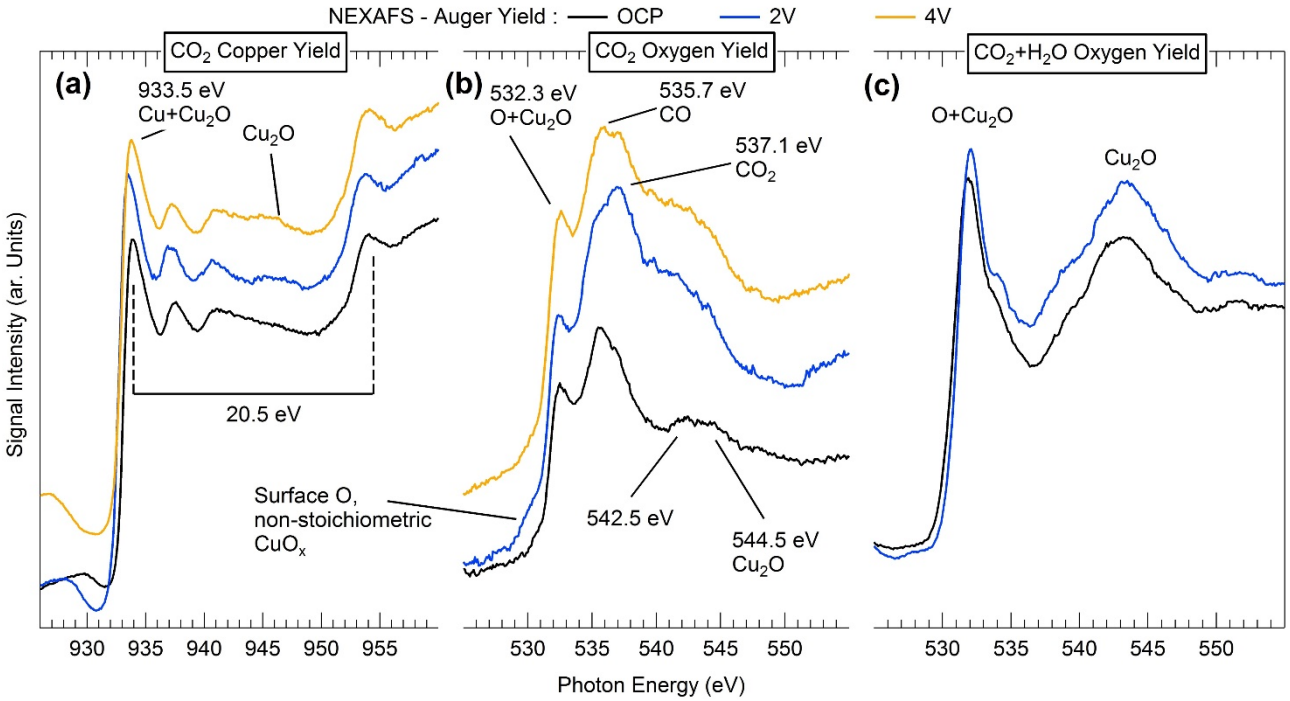

Figure 5 – NEXAFS spectra (Auger yield) at the Cu L and O K edges, recorded at 600°C at the indicated potentials in 0.5 mbar CO_2 (Panels a and b) and CO_2+H_2O 1/1 (Panel c).

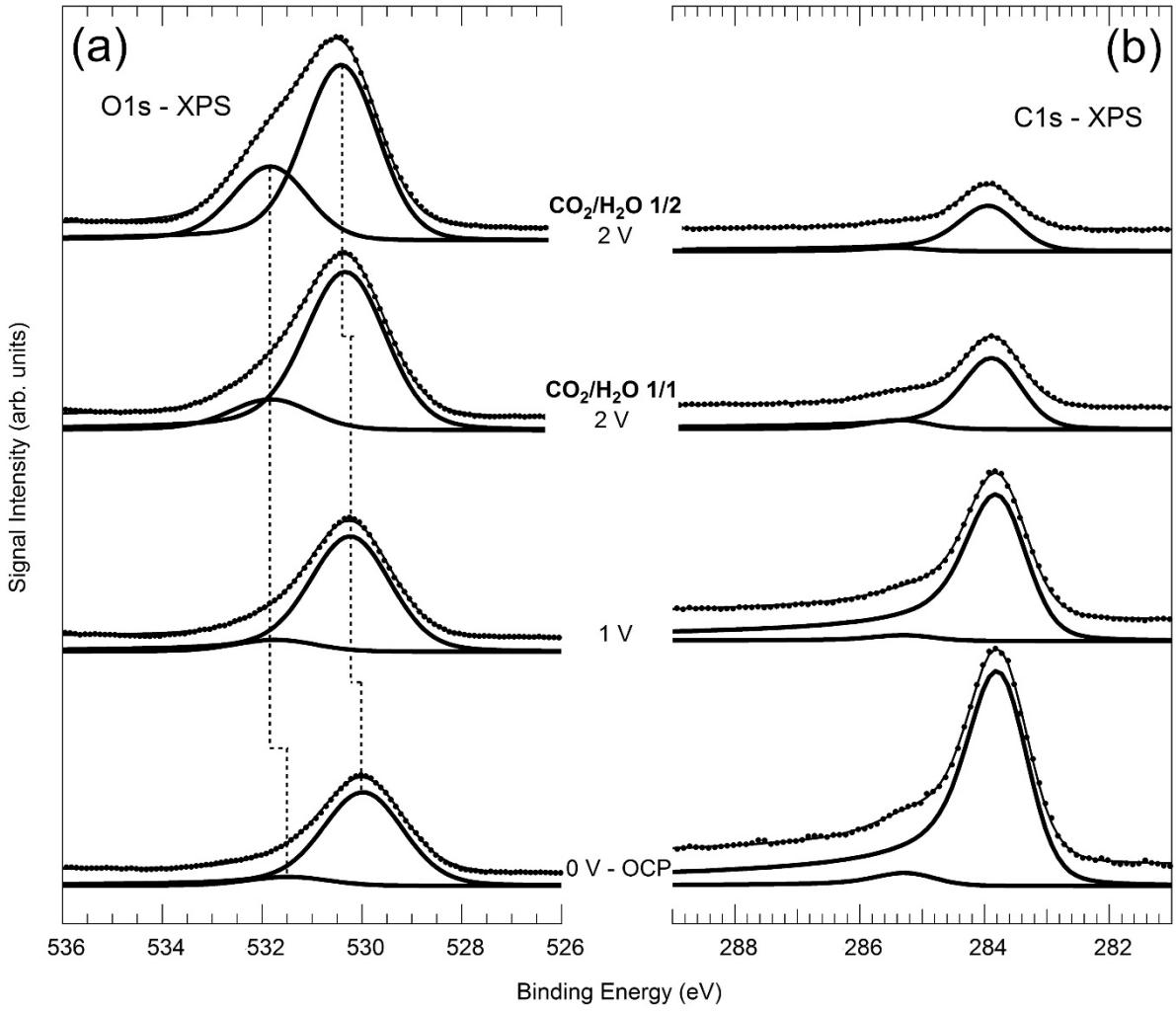

Figure 6 – (a) O 1*s* and (b) C 1*s* XPS spectra recorded in 0.5 mbar CO_2/H_2O 1/1 and 1/2 (see figure) at 600°C at the indicated potentials. The continuous lines are the results of the fitting procedure.

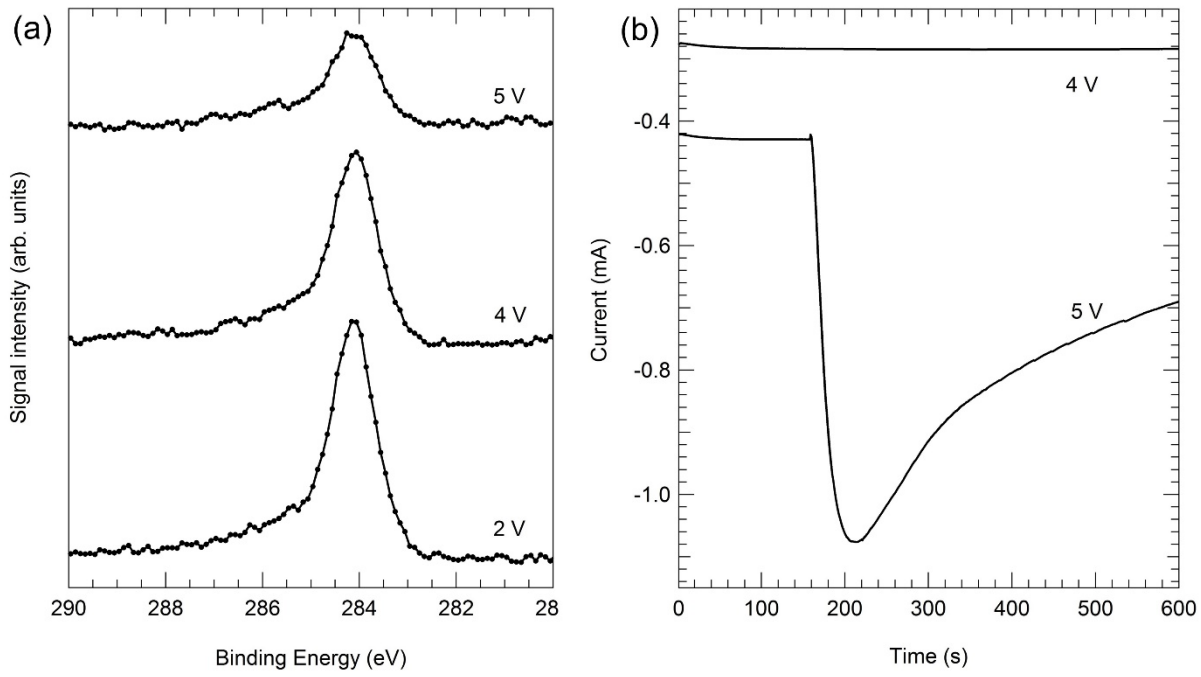

Figure 7 – Reductive C removal experiment in 0.5 mbar H_2O at 600°C at the Cu cathode. Electrode previously polarised potentiostatically at 2 V in 0.5 mbar CO_2/H_2O, as detailed in the text. (a) C 1s XPS spectra recorded at the indicated potentials: each potential has been applied for 5 min. (b) Potentiostatic transients recorded as a result of the application of the indicated cell polarisation, during the measurements of the C 1s XPS spectra shown in Panel (a).

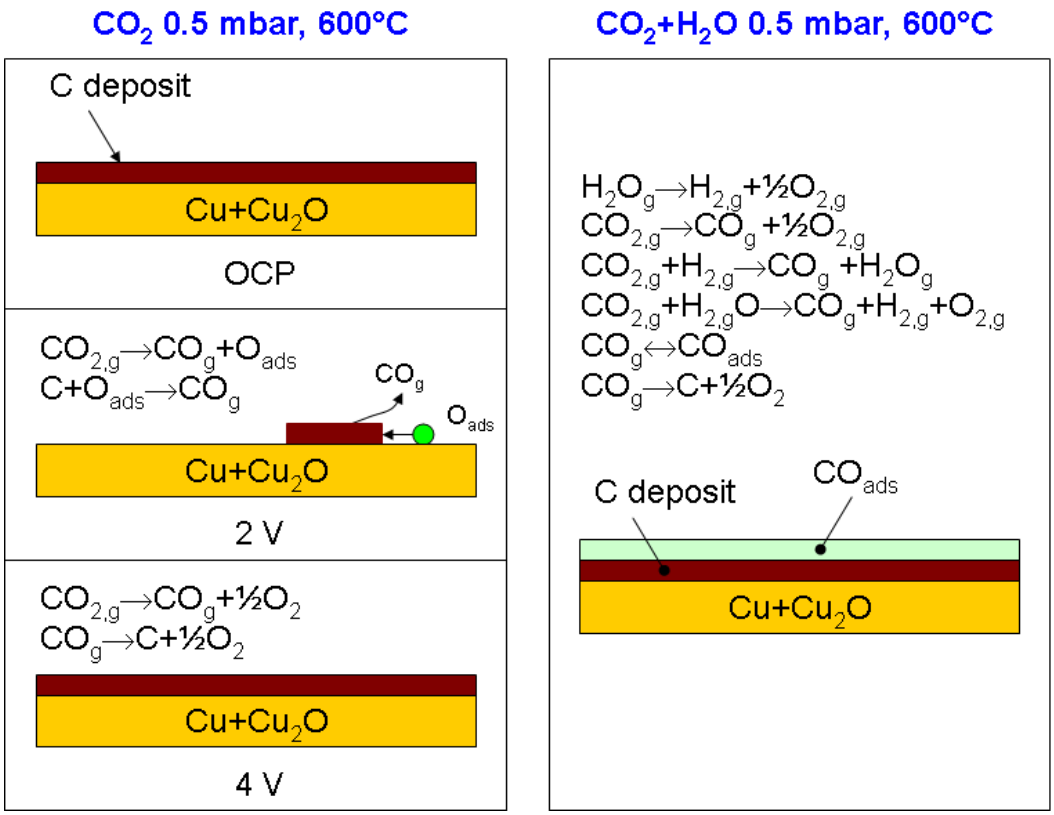

Figure 8 – Scheme of the reaction scenarios prevailing in the investigated gas environments under electrochemical polarisation.